NMR Solution Structure of Subunit F of the Methanogenic A_1A_O Adenosine Triphosphate Synthase and Its Interaction with the Nucleotide-Binding Subunit B[†,‡]

Shovanlal Gayen,[§,||] Subramanian Vivekanandan,[||] Goran Biuković,[§] Gerhard Grüber,*[,§] and Ho Sup Yoon*

School of Biological Sciences, Nanyang Technological University, 60 Nanyang Drive, Singapore 637551

Received June 5, 2007; Revised Manuscript Received August 16, 2007

ABSTRACT: The A_1A_O adenosine triphosphate (ATP) synthase from archaea uses the ion gradients generated across the membrane sector (A_O) to synthesize ATP in the A_3B_3 domain of the A_1 sector. The energy coupling between the two active domains occurs via the so-called stalk part(s), to which the 12 kDa subunit F does belong. Here, we present the solution structure of the F subunit of the A_1A_O ATP synthase from *Methanosarcina mazei* Gö1. Subunit F exhibits a distinct two-domain structure, with the N-terminal having 78 residues and residues 79−101 forming the flexible C-terminal part. The well-ordered N-terminal domain is composed of a four-stranded parallel β-sheet structure and three α-helices placed alternately. The two domains are loosely associated with more flexibility relative to each other. The flexibility of the C-terminal domain is further confirmed by dynamics studies. In addition, the affinity of binding of mutant subunit F, with a substitution of Trp100 against Tyr and Ile at the very C-terminal end, to the nucleotide-binding subunit B was determined quantitatively using the fluorescence signals of natural subunit B (Trp430). Finally, the arrangement of subunit F within the complex is presented.

Methanogens are able to grow by the conversion of a small number of compounds to methane. This rather simple pathway is not coupled to substrate-level phosphorylation but, instead, to the generation of ion gradients across the membrane. These ion gradients are used to drive the synthesis of adenosine triphosphate (ATP), catalyzed by the archaea type A_1A_O ATP synthases (A-ATP synthases (*1*)). Generally, the membrane-integrated enzyme is composed of subunits A−K in the stoichiometry of A_3:B_3:C:D:E:F:G:H_2:I:K_x (*2*). Like the related bacterial F_1F_O ATP synthase (F-ATP synthase) (α_3:β_3:γ:δ:ϵ:a:b_2:c_x) and the eukaryotic V_1V_O ATPase (V-ATPase) (A_3:B_3:C:D:E:F:G_2:H:a:d:c_x:$c_{x'}$:$c_{x''}$), it possesses a water-soluble A_1 domain, containing the catalytic sites, and an integral membrane A_O domain, involved in ion translocation (*3*−*6*). The primary structure of the archaeal ATP synthase is similar to that of the eukaryotic V-ATPase, but its function as an ATP synthase is more similar to that of the F-ATP synthases. ATP is synthesized or hydrolyzed on the A_1 headpiece, consisting of an A_3:B_3 domain, and the energy provided for or released during that process is transmitted to the membrane-bound A_O domain. The energy coupling between the two active domains occurs via the so-called stalk part(s) (*6*).

The A_1 ATPase, which is made up of the five different subunits A_3B_3CDF, is rather elongated in solution as revealed by small-angle X-ray scattering (SAXS) (*7*). The data show that the A_3:B_3 domain forms the headpiece, in which ATP cleavage takes place. The high-resolution structure of both nucleotide-binding subunits A (*8*) and B (*9*) have been determined previously. The A_3:B_3 sector is linked via an elongated stalk, formed by subunits C, D, and F in a stoichiometry of 1:1:1 (*10*), to the A_O sector. A comparison of the central stalk of this A_1 complex with bacterial F_1 and eukaryotic V_1 ATPases indicates different lengths of the stalk domain (*7*). Further insights into the topology of the A_1 ATPase were obtained from the 3D reconstruction of the A_1 complex, derived from single-particle analysis of electron micrographs (*10*) and biochemical approaches (*7*, *10*−*12*). These studies resulted in a model in which subunits C, D, and F form the central stalk domain (*10*−*12*). The first structure of the complete A_1A_O ATP synthase was obtained by single-particle analysis of negatively stained molecules (*13*, *14*). These studies revealed novel structural features such as two peripheral stalks and a collarlike structure, proposed to be composed of subunits H, I, and E, respectively (*13*, *14*). Recently, the high-and low-resolution structures of subunits E (*15*) and H (*16*), respectively, have been described.

Catalytic-site events (ATP synthesis and ATP hydrolysis) appear to be linked to ion translocation through conformational changes in the stalk-forming subunits. There is evidence from protein digestion studies (*11*) and cross-linking (*12*) that the F subunit changes conformation and/or moves between different sites in the A_1A_O ATP synthase complex during enzyme function. These important observations would be better understood if the structure of the F subunit and its location(s) in the A_1A_O complex were known. Most recently,

[†] S.G. is grateful to the authority of Nanyang Technological University for awarding a research scholarship. This research was supported by A*STAR BMRC (Grant 06/1/22/19/467).

[‡] The coordinates for the structure of subunit F have been deposited in BMRB with accession no. 15046 and the Protein Data Bank with code 2OV6.

* To whom correspondence should be addressed. (G.G.) Phone: 65-6316 2989. Fax: 65-6791 3856. E-mail: ggrueber@ntu.edu.sg. (H.S.Y.) Phone: 65-6316 2846. Fax: 65-6791 3856. E-mail: hsyoon@ntu.edu.sg.

[§] Section of Structure and Function of Molecular Motors.

[||] These authors contributed equally to this work.

10.1021/bi701102n CCC: $37.00
Published on Web 10/02/2007

the shape of subunit F of the A_1A_O ATP synthase from the archaeon *Methanosarcina mazei* Gö1 in solution was determined by SAXS, indicating that the protein is elongated and organized as two well-defined domains (*12*). Here we describe structural studies of the isolated F subunit of the A_1A_O ATP synthase from *M. mazei* Gö1 in solution using nuclear magnetic resonance spectroscopy. The dynamics of subunit F and its binding with the C-terminal domain of subunit B have been investigated.

EXPERIMENTAL PROCEDURES

Biochemicals. ProofStart DNA polymerase and Ni^{2+}−NTA[1] chromatography resin were received from Qiagen (Hilden, Germany); restriction enzymes were purchased from Fermentas (St. Leon-Rot, Germany). Chemicals for gel electrophoresis were received from Serva (Heidelberg, Germany). Bovine serum albumin was purchased from GERBU Biochemicals (Heidelberg, Germany). All other chemicals were at least of analytical grade and received from BIOMOL (Hamburg, Germany), Merck (Darmstadt, Germany), Roth (Karlsruhe, Germany), Sigma (Deisenhofen, Germany), or Serva (Heidelberg, Germany). $(^{15}NH_4)_2SO_4$ and (^{13}C)glucose were purchased from Cambridge Isotope Laboratories.

Cloning, Expression, and Protein Purification. Purification of subunits B, F, and H of the methanogenic A_1A_O ATP was performed as described in refs *9*, *12*, and *16*, respectively. For the production of uniformly labeled (^{15}N and ^{15}N/^{13}C) subunit F, the expressing bacteria were grown in M9 minimal medium containing $^{15}NH_4Cl$ or $^{15}NH_4Cl$/(^{13}C)-glucose.

To obtain the F mutant (*F*W100Y), with a substitution of Trp100 into a Tyr residue, the oligonucleotides with the sequences 5′-GTG ATT ATA CCA TGG AGT TAG CAG TG- 3′ (forward primer) and 5′ − AAT TGG AGC TCT TTA CTT CAT CAG ATC A- 3′ (reverse primer) have been used for amplification of the gene, encoding subunit F. The isoleucine mutant of subunit F (*F*W100I) was cloned using forward primer 5′ − GTG ATT ATA CCA TGG AGT TAG CAG TG- 3′ and reverse primer 5′-CTA TGA GCT CTT ACT TTA TCA GAT CAA CAC-3′. The restriction sites *Nco*I and *Sac*I were incorporated into the constructs. Following digestion with *Nco*I and *Sac*I, the pair PCR products were ligated into pET9d1−His_3. The cloned pET9d−His_3 vector containing the gene, encoding the subunit F mutants *F*W100Y and *F*W100I, respectively, was transformed into *Escherichia coli* cells (strain BL21) and grown on 30 μg/mL kanamycin-containing Luria−Bertoni (LB) agar plates. To express the protein mutants, liquid cultures were shaken in LB medium containing kanamycin (30 μg/mL) at 37 °C until an optical density (OD_{600}) of 0.6−0.7 was reached. To induce production of His_3−subunit F, the cultures were supplemented with isopropyl β-D-thiogalactoside (IPTG) to a final concentration of 1 mM. Following incubation for another 4 h at 30 °C, the cells were harvested at 10000*g* for 20 min, 4 °C. Subsequently, they were lysed on ice by sonication for 3 × 1 min in buffer A (50 mM Tris/HCl, pH 8.5, 100 mM NaCl, 4 mM Pefabloc SC (BIOMOL). The lysate was cleared by centrifugation at 10000*g* for 30 min at 4 °C, and the supernatant was passed through a filter (0.45 μm pore size) and supplemented with Ni^{2+}−NTA resin. The His-tagged protein was allowed to bind to the matrix for 90 min at 4 °C and eluted with an imidazole gradient (25−200 mM) in buffer A by mixing on a sample rotator (Neolab). Fractions containing *F*W100Y and *F*W100I were identified by SDS−PAGE (*26*), pooled, and subsequently applied to an ion-exchange column (Resource Q (6 mL), GE Healthcare), equilibrated in a buffer of 50 mM Tris/HCl (pH 8.5) and 100 mM NaCl.

The purity of the protein sample was analyzed by SDS−PAGE (*26*). Protein concentrations were determined by the bicinochonic acid (BCA) assay (Pierce, Rockford, IL).

NMR Data Collection and Processing. The NMR sample was prepared in 90% H_2O/10% D_2O containing 25 mM NaH_2PO_4/Na_2HPO_4 (pH 6.5) and 0.1% NaN_3. All NMR experiments were performed at 288 K on Bruker Avance 600 and 700 MHz spectrometers equipped with 5 mm triple-resonance (^{1}H/^{15}N/^{13}C) single-axis gradient probes and a cryoprobe for both the spectrometers. Matrix-assisted laser desorption ionization/time-of-flight mass spectrometry has been performed after data collection to confirm the absence of protein degradation during the NMR experiment. Homonuclear experiments included 2D ^{1}H, ^{1}H nuclear Overhauser effect spectroscopy (NOESY), and total correlation spectroscopy (TOCSY) experiments for samples in H_2O and ^2H_2O (spectral widths of about 9615.85 Hz in both dimensions, using a WATERGATE scheme to suppress the water signal for the H_2O samples and presaturation of the residual water signal during recovery time for the ^2H_2O samples). Heteronuclear experiments included 2D ^{15}N heteronuclear single-quantum correlation (HSQC), 2D ^{13}C HSQC, 3D HNCA, HNCO, HN(CO)CA, HNCACB, CBCA(CO)NH, HNCACO, HCCH-TOCSY, HCCCONH, 3D ^{15}N NOESY−HSQC, and 3D ^{13}C NOESY−HSQC. In all the above experiments, spectral widths were generally 9.6 kHz for protons and 2.8 kHz for ^{15}N, while for ^{13}C dimensions they were 6−12 kHz. A 3D ^{15}N−^{1}H NOESY−HSQC and 3D ^{13}C−^{1}H NOESY−HSQC mixing time of 100 ms was used for NOESY assignment. All three-dimensional experiments made use of pulsed-field gradients for coherence selection and artifact suppression and utilized gradient sensitivity enhancement schemes. Quadrature detection in the indirectly detected dimensions was achieved using either the States/TPPI (time-proportional phase incrementation) or the echo/antiecho method. Baseline corrections were applied wherever necessary. The proton chemical shift was referenced to the methyl signal of 2,2-dimethyl-2-silapentane-5-sulfonate (Cambridge Isotope Laboratories) as an external reference at 0 ppm. The ^{13}C and ^{15}N chemical shifts were referenced indirectly to DSS. All the NMR spectra were processed using either nmrPipe/nmrDraw or Bruker Avance spectrometer in-built

[1] Abbreviations: EDC, 1-ethyl-3-[(dimethylamino)propyl]carbodiimide; ϵ, subunit ϵ of the F-ATP synthase (*23*); F_{Tt}, subunit F of the prokaryotic V-ATPase from *Thermus thermophilus*, F_{Mm}, subunit F of the A-ATP synthase from *Methanosarcina mazei* Gö1; HSQC, heteronuclear single-quantum coherence; IPTG, isopropyl β-D-thiogalactoside; NMR, nuclear magnetic resonance; NOE, nuclear Overhauser effect; NOESY, NOE spectroscopy; NTA, nitrilotriacetic acid; PAGE, polyacrylamide gel electrophoresis; PCR, polymerase chain reaction; SAXS, small-angle X-ray scattering; R_1, longitudinal relaxation time; R_2, transversal relaxation time; RMSD, root mean square distance; SDS, sodium dodecyl sulfate, TOCSY, total correlation spectroscopy; T_1, longitudinal relaxation time; T_2, transverse relaxation time; Tris, tris(hydroxymethyl)aminomethane; DTT, dithiothreitol; EM, electron microscopy.

software Topspin. Peak-picking and data analysis of the Fourier-transformed spectra were performed with the SPARKY program (*27*).

NMR Spectroscopy and Structure Calculation. The additional His residues of the His tag at the N-terminus, which are essentially unstructured, were not used in the structure calculation. The structure calculation was performed starting from first methionine in the N-terminal which is after the proline residue. The ^{1}H sequential assignment was achieved mainly using homonuclear 2D NOESY (ι_m = 100 ms) and TOCSY spectra in both H_2O and ^2H_2O solutions at 600 MHz and 288 K; this approach was adopted because labeled protein samples only became available later in the work. Once labeled protein was available, assignments were extended to include backbone ^{15}N and ^{13}C signals using ^{15}N NOESY−HSQC, ^{13}C NOESY−HSQC, and triple-resonance backbone experiments (HNCACB, CBCA(CO)NH). All side chain assignments were made using HCCH-TOCSY, HCCCONH, and (H)CCCONH experiments, again in combinations with 2D NOESY and TOCSY data. The distance restraints for the structure calculation were collected from 3D ^{15}N−^{1}H NOESY−HSQC and ^{13}C−^{1}H NOESY−HSQC by manual and automatic assignments for which CYANA 2.1 was used. To minimize the effects of spin diffusion, intraresidue and sequential NOE intensities were obtained from 100 ms NOESY spectra. Dihedral angle restraints were calculated from chemical shifts using torsion angle likelihood obtained from shift and sequence similarity (TALOS) (*28*) and over all secondary structures were predicted from the chemical shift index (CSI) (*30*) and NOE pattern. The upper bound for all NOE distance restraints was initially set to 5 Å and adjusted for nonstereospecifically assigned methylene and methyl protons using the method described originally for DYANA and detailed by Guntert (*31*). Experimental evidence for hydrogen bonds was obtained from hydrogen/deuterium exchange in perdeuterated buffer at 288 K over a period of 24 h. The structure calculations were performed with the CYANA 2.1 program package (*32*), which uses simulated annealing in combination with molecular dynamics in torsion angle space. At the first round of structure calculations, only unambiguous long-range NOE constraints were used to generate a low-resolution fold for the structure. Assignments of ambiguous NOE cross-peaks were made by applying a structure-aided filtering strategy in repeated rounds of structure calculations. The 15 residues starting from Ser80 to Gly94 were completely lacking intra- and interresidue NOEs and were assumed to be unobservable due to rapid exchange with solvent. This region of the protein is entirely unstructured as no chemical shift resonances were made possible from the 3D ^{15}N NOESY−HSQC and 3D ^{13}C NOESY−HSQC spectra. Starting ab initio, 100 conformers were calculated in 8000 annealing steps each. The program MOLMOL (*33*) was used to visualize the result of ensemble of minimized conformers.

Correlation Time (τ_c) and Relaxation Measurements. The correlation time of the F subunit was estimated using the equation

$$\tau_c = \{[6(T_1/T_2) - 7]/4\}^{1/2}/\Omega_N 2\pi$$

where T_1 and T_2 are the mean longitudinal and transverse relaxation times for the structured residues (residues 1−80) of the F subunit and Ω_N is the Larmor frequency of ^{15}N at the field strengths of 14.1 and 16.4 T used here. The ^{15}N longitudinal and transverse relaxation time constants, T_1 and T_2, respectively, were determined by collecting a time series of ^{15}N HSQC spectra with sensitivity enhancement. ^{15}N relaxation measurements were acquired on Bruker Avance 600 and 700 MHz spectrometers equipped with a cryoprobe at a temperature of 288 K using the triple-axis gradient-enhanced and sensitivity-enhanced ^{1}H−^{15}N HSQC experiment provided in the Bruker pulse sequence library.

For T_1 measurements, the spectra were collected with relaxation delays of 5, 40, 80, 130, 210, 330, 470, 630, 800, and 1000 ms, with repeat experiments at 40 and 130 ms for error estimations. For T_2 measurements, data were acquired with delays of 14.4, 28.8, 43.2, 57.6, 72.0, 86.4, 100.8, 115.2, 129.6, 144.0, and 158.4 ms with duplicate points at 43.2 and 72.0 ms. The delay between 180 pulses in the Carr−Purcell−Meiboom−Gill (CPMG) pulse train for T_2 measurements was fixed at 0.9 ms. A total of 2048 complex data points with 128 complex increments were collected for the relaxation experiments. The relaxation rate constants were determined by fitting the cross-peak intensities to a monoexponential function.

T_1 and T_2 spectra were recorded with spectral widths of 9615.85 Hz sampled over 2048 complex points in the ω_2 (^{1}H) dimension and 2405.12 Hz over 128 complex points in the ω_1 (^{15}N) dimension with 16 scans for each increment in the indirect dimension. The relaxation delay for both T_1 and T_2 measurements was 1.5 s.

The heteronuclear steady-state NOE spectra were acquired with spectral widths of 9615.85 Hz over 2048 complex points in the ω_2 (^{1}H) dimension and 2405.12 Hz over 128 complex points in the ω_1 (^{15}N) dimension. ^{15}N decoupling during acquisition was achieved using a GARP-4 pulse sequence (*34*). The field strength of the CPMG refocusing train was about 3.3 kHz, and a 1.2 ms delay was used between the refocusing pulses (*35*). To compensate the temperature difference between the experiments, a series of off-resonance pulses was applied at the very beginning of the pulse sequence on the ^{15}N channel. The CPMG duration was kept in such a way that it had to last long enough to observe a significant effect on the peaks observed and short enough for us to be able to observe these peaks. The optimal value for F was found to be 35 ms. The values of two different frequencies of ν_{CPMG}^{min} and ν_{CPMG}^{max} were used to determine the conformational mobility (*36*, *37*). The reference spectra were collected at these two different frequencies without the relaxation delay performed at the beginning and at the end of the series. The effects of cross-relaxation between ^{15}N−^{1}H dipolar and ^{15}N chemical shift anisotropy were removed by applying 180° pulses during relaxation delay (*34*). Values of R_2(CPMG) were calculated from the following relation: $R_2(\mathrm{CPMG}) = (-1/T)\ \ln(I(\nu_{CPMG})/I_o)$, where R_2(CPMG) is the transverse relaxation constant, T is the length of the relaxation delay, $I(\nu_{CPMG})$ is the intensity of the peak at the corresponding minimum and maximum of the ν_{CPMG} frequency, and I_o is the intensity of the same peak on the reference spectrum (*37*).

To allow NOE evolution, ^{1}H−^{15}N steady-state NOE values were measured with two different data sets, one collected

with no initial proton saturation and a second with initial proton saturation. The proton saturation period was 3 s.

For the determination of the H/D exchange factors, the F subunit sample was lyophilized and resuspended in 100% D_2O. A series of 2D $^1H-^{15}N$ HSQC spectra were obtained immediately after the lyophilized protein was dissolved in 0.5 mL of ^2H_2O. The dead time of the experiment was about 30 min.

Data Processing and Analysis. The HSQC spectra were processed using nmrPipe software (*38*). Peak-picking and data analysis of the Fourier-transformed spectra were performed with the SPARKY program (*39*). The T_1 and T_2 spectra were processed using a sine bell apodization function shifted by 90° for both dimensions. The final sizes of the matrices were 2048 × 128 real points after zero filling in both the dimension and the Fourier transformation. An automated baseline correction was applied in both dimensions. The spectra were referenced to the DSS signal (*40*).

T_1 and T_2 values were obtained by fitting the peak intensities using single-exponential decay:

$$I(t) = I_0 \exp(-t/T_{1,2})$$

where $I(t)$ is the peak intensity, t is the time, and I_0 is the intensity at time 0.

The heteronuclear steady-state $^{15}N-^1H$ NOE values were obtained from the ratios of the peak intensities in the saturated spectrum to those in the unsaturated spectrum. To suppress time- or temperature-dependent effects, the spectra were acquired in an interleaved mode with incremented relaxation delays. All experiments were recorded with 256 t_1 increments of 2048 data points in t_2. The spectral widths were set to 9586.15 Hz (^1H) and 2406 Hz (^{15}N) at 600 MHz. Errors were estimated by evaluating the standard deviation of the NOE, σ_{NOE}:

$$\sigma_{NOE}/NOE = (\sigma I_{sat}/I_{sat})^2 + (\sigma I_{unsat}/I_{unsat})^{21/2}$$

where σI_{sat} and σI_{unsat} are the standard deviations of the noise in the spectra (*41*).

Fluorescence Measurements. A Varian Cary Eclipse spectrofluorimeter was used, and all experiments were carried out at 20 °C. The samples were excited at 295 nm, and the emission was recorded from 310 to 380 nm with excitation and emission band-passes set to 5 nm. For titration of the tryptophan fluorescence of subunit B with subunit F mutants *F*W100Y and *F*W100I and subunit H, the emission wavelength was 338 nm. Before use, subunit B and increasing amounts of *F*W100Y were incubated in a buffer of 50 mM Tris/HCl (pH 8.5) and 150 mM NaCl for 20 min.

RESULTS

Resonance Assignments of the F Subunit of the A_1A_O ATP Synthase. The assignments of the resolved backbone residues of the F subunit are presented on a 2D $^1H-^{15}N$ HSQC spectrum (Figure 1). The HSQC peaks were identified for all residues except for Phe15, and Gly83, Ser84, Glu89, and Asp98, which are present in the flexible C-terminal domain. The amides of these residues undergo fast exchange with the solvent and were not observable in the HSQC as they reside in the flexible loop region. The absence of the N-terminal Phe15 amide resonance could be due to the high solvent exchange rate at this region of the helix.

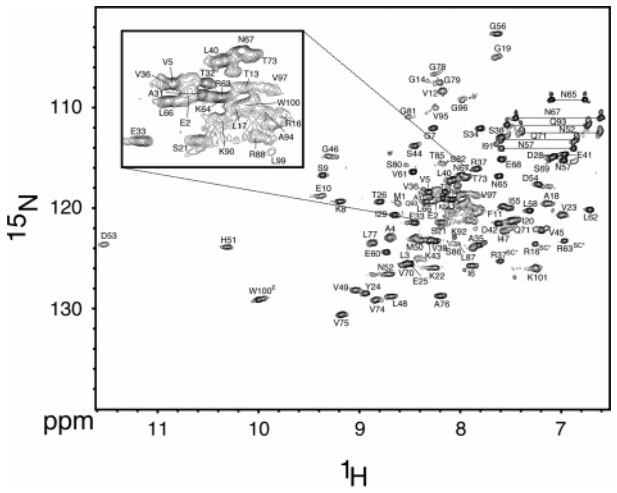

FIGURE 1: $^1H-^{15}N$ HSQC spectrum of subunit F of the methanogenic A_1A_O ATP synthase in 25 mM sodium phosphate buffer (pH 6.5) at 288 K. Backbone and side chain (sc) amide assignments are shown for each residue. HSQC cross-peaks of side chain residues R16, R37, and R63 are folded in the ^{15}N dimension and indicated by "SC*". Signals from side chain NH_2 groups are connected by horizontal lines. The overlapping region is expanded and marked by dashed lines.

Despite showing a well-dispersed $^1H-^{15}N$ HSQC spectrum, the F subunit exhibited different line widths for a significantly large number of residues. To examine this phenomenon further, we recorded HSQC spectra at various concentrations ranging from 0.1 to 1 mM, showing no measurable differences either in the line widths or in the chemical shifts of ^1H and ^{15}N resonances (data not shown). As shown by SAXS (*12*) the protein is indeed monomeric in solution at the concentration used, indicating that the broadness of the peak in the 2D HSQC is due to the conformational exchange, altering the environment of a nuclear spin and modulating its chemical shift. When this process is on the microsecond to millisecond time scale and the chemical shift changes are large, the NMR signal broadens. The conformational exchange is indicated by extensive broadening of the NMR spectra. Three different types of line shapes of the peaks were observed in the HSQC spectrum. There are single intense peaks and single peaks with exchange broadening, and two or more peaks appear with skewed populations (Supporting Information Figures S2 and S3). Interestingly, all the intense peaks are found to be clustered in the middle of the protein sequence representing residues in β2, α2, β3, α3, and β4 (Supporting Information Figure S4). The intensities of the peaks are very low for the C-terminal residues, indicating that this region is flexible compared to the N-terminal domain. This difference in intensity of HSQC peaks is clear evidence that the protein undergoes conformational exchange on the microsecond to millisecond time scale. In addition, the presence of Gly and Ser in the C-terminus favors a disordered structure, and this could also contribute to the missing chemical shift resonances in the C-terminal domain.

Solution Structure of the F Subunit of the A-ATP Synthase. The structure of the F subunit (F_{Mm}) was calculated on the basis of a total of 1399 nontrivial NMR-derived distance

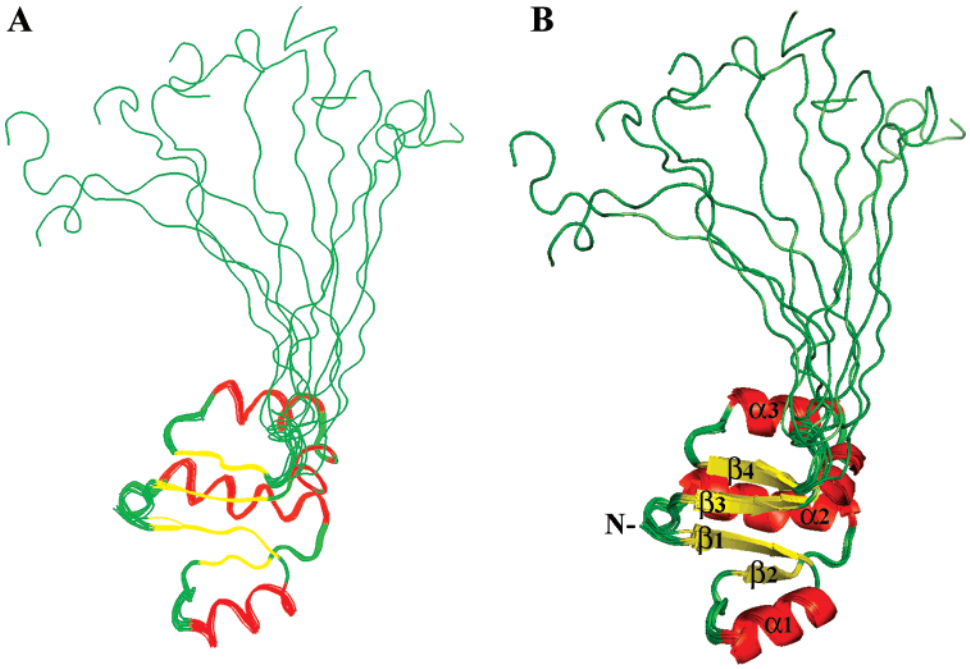

FIGURE 2: Backbone (N, C_α, C′) (A) and ribbon (B) diagrams of 10 low-energy NMR-derived structures of subunit F of the A_1A_O ATP synthase from *M. mazei* Gö1. This figure was produced using MOLSCRIPT (*42*).

Table 1: Structural Statistics for the 10 Selected Structures of Subunit F of Methanogenic A_1A_O ATP Synthase after Energy Minimization

total number of NMR restraints	1399
number of unambigous NOE peaks	
intraresidue ($i = j$)	301
sequential ($\|i - j\| = 1$)	377
medium-range ($2 \leq \|i - j\| \leq 4$)	261
long-range ($\|i - j\| > 4$)	297
number of dihedral angle constraints	163
number of hydrogen-bond distance restraints	16
number of restraint violations[a]	
total number of restraint violations >0.5 Å	0
total number of dihedral angle violations >5°	0
Ramachandran plot[b]	
fraction of residues in most favored regions (%)	70.6
fraction of residues in additionally allowed regions (%)	28.9
fraction of residues in generously allowed regions (%)	0.4
fraction of residues in disallowed regions (%)	0.1
average RMSD to mean (Å)	
backbone (residues 1−78)	0.39 ± 0.09
heavy atoms (residues 1−78)	0.78 ± 0.08

[a] There are no distance violations greater than 0.5 Å or dihedral angle violations greater than 5°. All residues are included in the final ensemble. [b] The Ramachandran plot was for all the residues.

restraints. Figure 2 shows an overlay of the 10 lowest energy structures of F, and the statistics are given in Table 1. These structures have an overall RMSD of 0.39 ± 0.09 Å for backbone atoms and 0.78 ± 0.08 Å for all heavy atoms in the well-ordered regions of the three-dimensional structures (residues 1−78) of the protein. All these structures have energies lower than 3.7 kcal mol^{-1}, no NOE violations greater than 0.3 Å, and no dihedral violations greater than 5°. The protein has both α-helices and *β*-strands in its tertiary structure as evidenced by the location of relevant NOE restraints (see Supporting Information Figure S1). The solution structure of subunit F is divided into a well-defined N-terminal domain, formed by an α/*β* fold, and an extended C-terminal tail at its very end (Figure 2). The four strands of the *β*-sheet of the N-terminal part are oriented parallel to each other and are separated due to the three α-helices (α1−α3). These α-helices are made up by residues Ser9−Ala18, Ala31−Val39, and Val61−E68, whereas residues Leu3−Gly7, Lys22−Thr26, Val45−Asn52, and Thr73−Ala76 form the *β*-strands (*β*1−*β*4). The dimensions of the elongated F subunit (78.7 Å) are approximately 24.2 Å × 28.5 Å × 38.7 Å for the N-terminal part. The C-terminal tail has a length of about 40 Å.

Intramolecular Dynamics of the C-Terminal Domain. A first indication that the N- and C-terminal domains of the F subunit are in loose contact in the solution structure is the observation that there are no long-range NOEs between residues of the N- and C-terminal domains. The backbone $^{15}N\{^1H\}$ NOE data show that the peaks in the C-terminal regions are weakened, indicating that the two domains of the F subunit tumble as two different entities (Figure 3A). High RMS deviations of the C-terminal domain of the F subunit reflect underdetermination due to the lack of distance and dihedral restraints. Also, residues in this domain have very few observable NOEs because they are located in regions with backbone flexibility. Figure 3B−D, F−H illustrates the R_1 and R_2 relaxation rate constants and R_2/R_1 ratios measured at two different field strengths of 14.1 and 16.4 T, respectively. There is a discernible increase in R_1, and a decrease in the R_2 values is observed in the C-terminal end of the protein (around 20 amino acids). The average values of the relaxation parameters R_1 and R_2 and NOEs in the ordered regions (residues 1−78) calculated at 14.6 and 16.4 T are 1.104, 23.469, and 0.774 s^{-1} and 1.174, 16.334, and 0.809 s^{-1}, respectively (Figure 3. Taken together, the data clearly indicate that the C-terminal end of the protein experiences conformational mobility compared to the rest of the protein.

Overall correlation times of 14.5 ns for 14.6 T and 9.94 ns at 16.4 T were obtained for this F subunit protein according to the equation described in the Experimental Procedures. To examine further the presence of conforma-

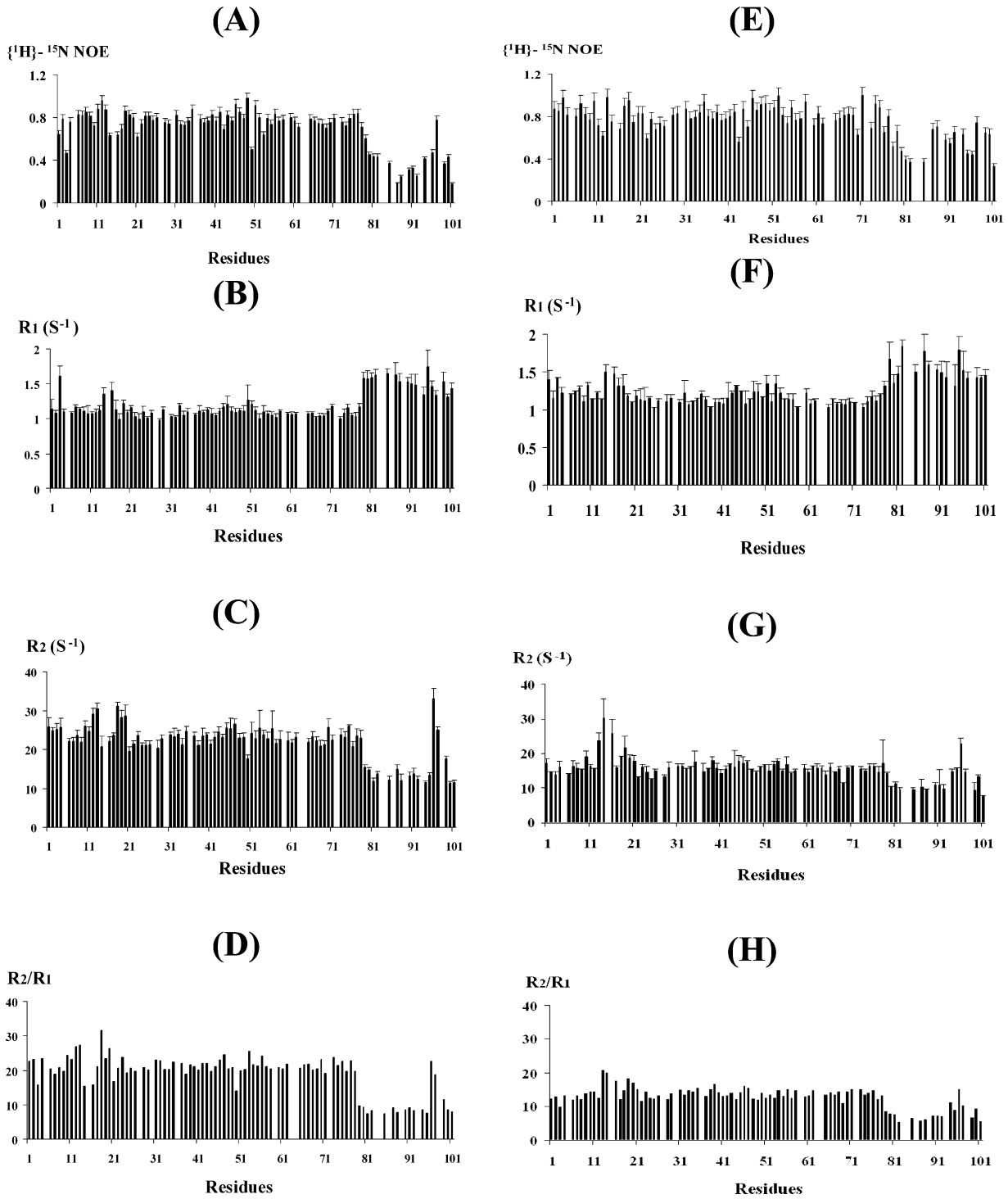

FIGURE 3: Comparison of NMR data collected on 600 MHz (A−D) and 700 MHz (E−H) spectrometers. (A, E) Steady-state $\{^1H\}-^{15}N$ NOE enhancement data. The less intense bar graph indicates that this portion (80−101) of the protein is very dynamic. (B−D, F−H) Experimental longitudinal (R_1) and transverse (R_2) ^{15}N relaxation rates and R_2/R_1 ratios obtained for subunit F_{Mm} at 600.13 and 700.13 MHz, respectively. Almost all residues in the well-ordered region exhibit a rather uniform dynamic behavior, suggesting low backbone mobility for this region (1−78) of the protein structure. All C-terminal residues show a rather nonuniform dynamic behavior, suggesting high backbone mobility for this C-terminal region of the protein structure. The error bars represent the SD.

tional exchanges on the micro- to millisecond time scale in subunit F, a rough estimation of the amount of conformational motions in the backbone of subunit F has been made from the difference in the R_2 values obtained for the two extreme values of $\nu_{CPMG}^{min} - \nu_{CPMG}^{max}$ (*35*, *36*). As shown in Figure 4, a difference between the two experiments was observed in a number of residues in subunit F with significant positive values of $R_2(\nu_{CPMG}^{min}) - R_2(\nu_{CPMG}^{max})$, indicating conformational exchange occurs at multiple backbone sites in the protein. The corresponding residues probed by CPMG experiments were located primarily in the three different regions of the protein, in the N-terminal, loop 1−α1−loop 2 (residues 8−23), in the middle part, β3−loop 3 (residues 47−53), and in β4 (residues 75, 76, and 79) and the C-terminal part of subunit F, suggesting a chemical exchange phenomenon in these regions.

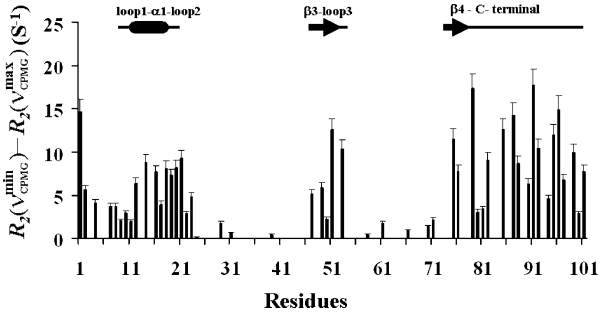

FIGURE 4: Conformational exchange in subunit F of the methanogenic A_1A_O ATP synthase. Measurement of backbone conformational motions from the difference values of R_2(CPMG) at minimal and maximal CPMG pulse repetition rates. $R_2(\nu_{CPMG}^{min}) - R_2(\nu_{CPMG}^{max})$ are displayed as a function of the F subunit sequence. Positive values are expected for residues that undergo conformational exchange.

Fluorescence Titration of Subunit B with the Subunit F Mutant FW100Y. Previous work has shown that the C-terminal peptide I82−R90 of subunit F and the C-terminal region D388−R402 of the nucleotide-binding subunit B of the methanogenic A_1A_O ATP synthase can be cross-linked (*12*), suggesting that these peptides, or the region around them, might be in close proximity. The sequence of subunit F has only one Trp residue (Trp100), which is located at the C-terminal end (*17*). This Trp has been substituted by a Tyr residue in the mutant *F*W100Y and subjected to measurement of binding characteristic of the nucleotide-binding subunit B under more physiological protein concentrations. As demonstrated in Figure 5A the mutant protein does not show Trp intensity in the fluorescence spectrum. Subunit B contains one native Trp (Trp430), which is at the C-terminal region of the structure (Figure 7; *9*) and thereby close to the C-terminal peptide involved in the B−F cross-link formation. The corrected tryptophan fluorescence spectrum of subunit B shows the emission maximum of the protein at 339 nm (Figure 5A). The intensity dropped by 19% after addition of the mutant *F*W100Y. By comparison, when subunit B was incubated with a mutant, in which Trp is exchanged by an Ile residue (*F*W100I), a fluorescence quenching of only

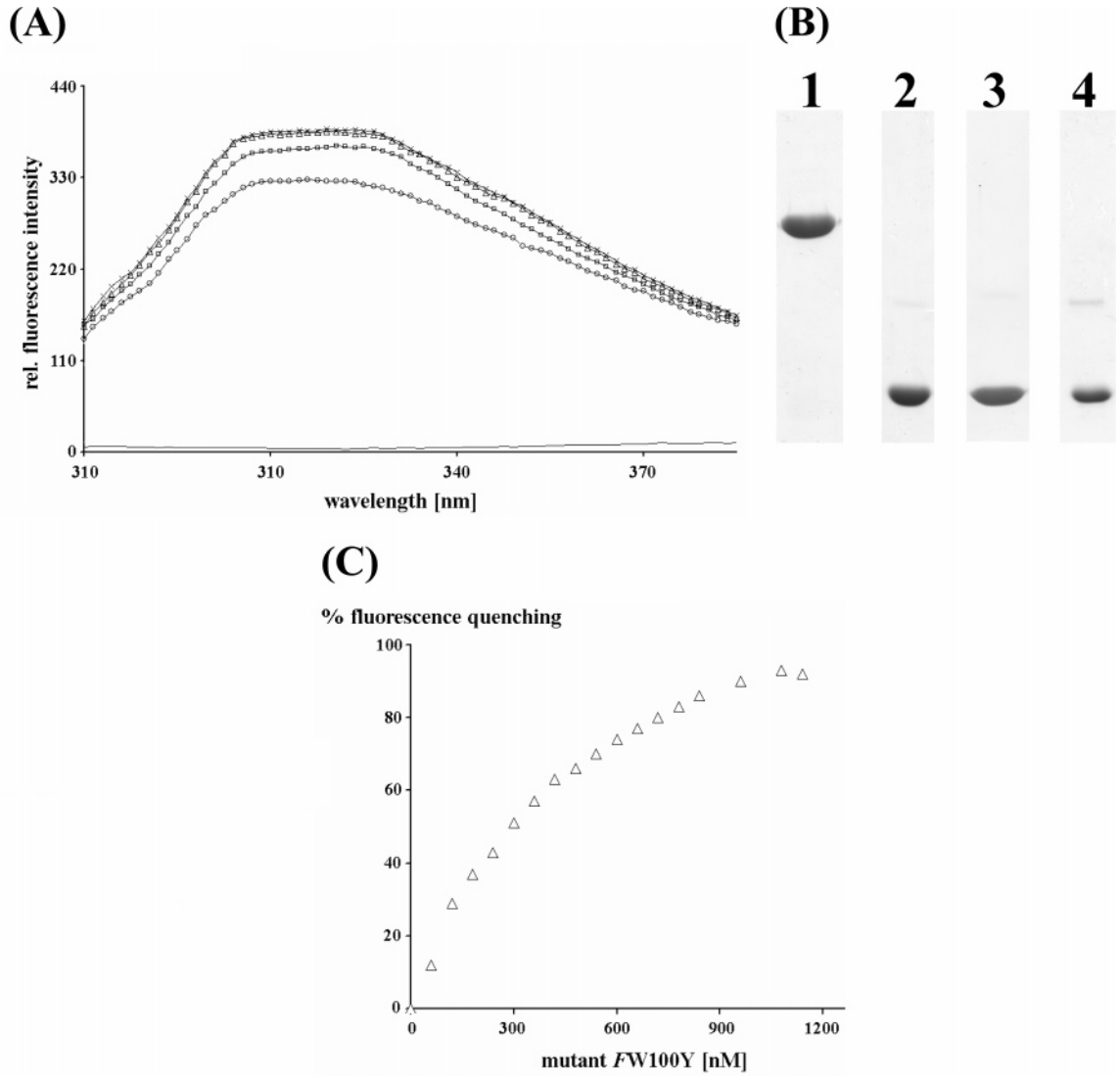

FIGURE 5: Tryptophan fluorescence spectra of subunit B (Δ) and binding of the F subunit mutant *F*W100Y to subunit B (1 μM) (C). (A) The emission spectra were recorded 20 min after addition of mutant *F*W100Y (○), mutant *F*W100I (□), and subunit H (+) of the methanogenic A_1A_O ATP synthase from *M. mazei* Gö1 using $\lambda_{ex} = 295$ nm with emission and excitation slits at 5 nm. (B) The SDS gel shows a sample of the expressed and purified subunit B (lane 1), mutants *F*W100Y (lane 2) and *F*W100I (lane 3), and subunit H (lane 4) used in the fluorescence spectroscopy measurement. Subunit B was incubated with subunit H, mutant *F*W100Y, and mutant *F*W100I for 15 min each on ice. (C) Fluorescence titration of subunit B with the mutant *F*W100Y. Excitation was at 295 nm, and emission was measured at 338 nm.

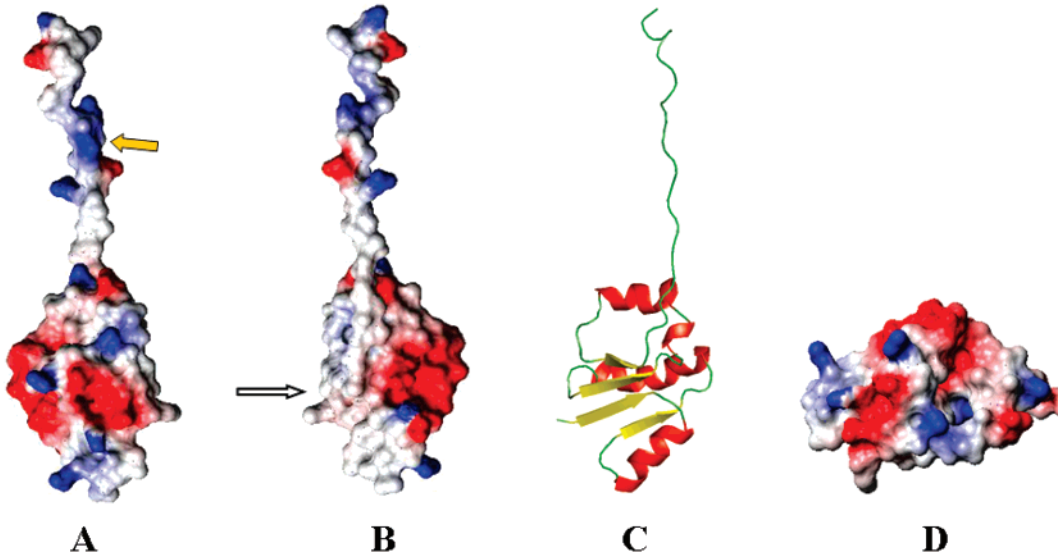

FIGURE 6: Charge distributions on the surfaces of subunit F of the methanogenic A_1A_O ATP synthase. Red and blue areas are negatively and positively charged areas, respectively, calculated with the program MOLMOL (*32*). At the left (A) the arrow shows the positively charged tail, which forms a cross-link with the C-terminus of subunit B (*12*). The hydrophic area, which is proposed to interact with the central subunit D, is emphasized by a white arrow (B). A ribbon representation of the F subunit in an orientation similar to that of the surface structure is shown in (C). (D) Surface representation of the N-terminal domain from the membrane side.

5% was observed. These data indicate that the significant drop in fluorescence intensity shown for the case of *F*W100Y is mainly caused by the interaction of Trp430 of subunit B and the aromatic Tyr residue of the mutant *F*W100Y. In a control experiment the peripheral stalk subunit H of the A_1A_O ATP synthase, lacking any aromatic residue (*16*), has been incubated with subunit B, resulting in a spectrum identical to that of subunit B (Figure 5A). To quantitatively evaluate the spectra, the binding of the mutant *F*W100Y to B was measured using the fluorescence quenching at 339 nm, and the result is shown in Figure 5C. The titration curve has a hyperbolic shape from which a binding constant (K_d) of 322 nM could be determined, with the assumption of a B to F ratio of 1:1.

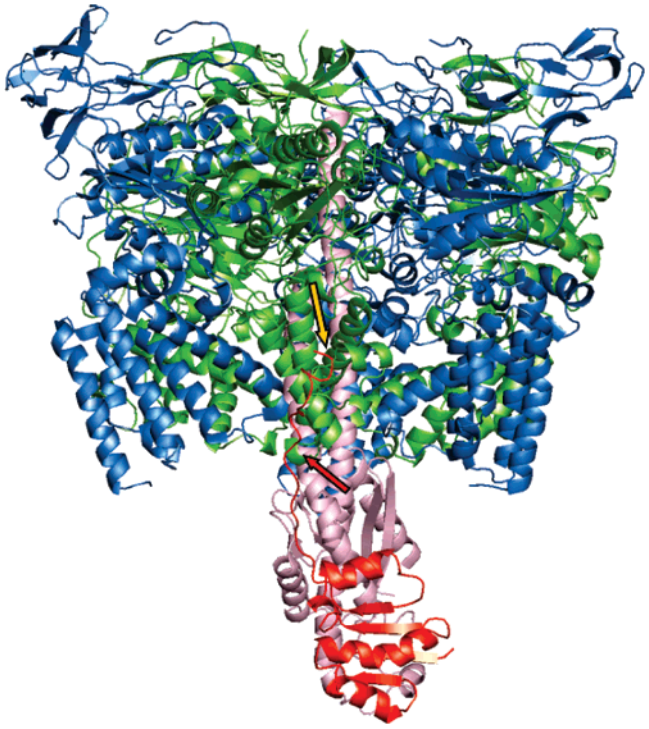

FIGURE 7: Proposed binding of subunit F inside the A_3B_3DF complex of the A_1 ATPase. *Pyrococcus horikoshii* A-ATP synthase subunit A (pink, PDB code 1vdz; *8*) and *M. mazei* Gö1 A-ATP synthase subunit B (green, PDB code 2c61; *9*), as well as the bovine mitochondrial F-ATP synthase γ subunit (violet, PDB code 1e1q, chain G; *43*), which is homologous to subunit D of the A-ATP synthase, were fitted into the electron density map of the A_1 ATPase (*10*) and A_1A_O ATP synthase (*14*), obtained from single-particle analysis electron micrographs (*9*). The solution structure of subunit F of the *M. mazei* Gö1 A-ATP synthase is highlighted in red. The yellow and red arrows indicate the intrinsic Trp residue (Trp430) of subunit B and the contact region of subunits B and F, respectively. The figure was prepared using PyMOL (http://www.pymol.org).

DISCUSSION

The dual function of ion transport and ATP synthesis or ATP hydrolysis of the A_O and A_1 domains of the entire A_1A_O ATP synthase reflects a complicated coupling process during enzyme reaction. High-resolution crystal structures are available for the catalytic and nucleotide-binding subunits A (*8*) and B (*9*) of the A-ATP synthase, respectively, providing information on the nucleotide-binding events. The situation is different with regard to the structure of the central stalk subunits, which form the primary coupling element. Those subunits undergo conformational changes and/or rearrangements. Therefore, knowledge of their structure is essential for understanding their molecular mechanisms and biological roles. The shape of the hydrated stalk subunit F (F_{Mm}) of the A_1A_O ATP synthase from *M. mazei* Gö1 in solution, determined by SAXS, showed that the protein is a monodisperse and elongated particle (75.0 Å), supported by exclusion chromatography (*12*). The solution structure of F_{Mm} presented here is similar in dimension (78.7 Å) and shape and is organized as two well-defined domains. The elongated fashion of this structure enables this subunit to function as a coupling element by connecting the nucleotide-binding subunit with the ion-translocating part. This is supported by the fact that subunit F can be cross-linked to subunit B inside the methanogenic A_3B_3DF subcomplex (*11*), A_1 ATPase (*10*),

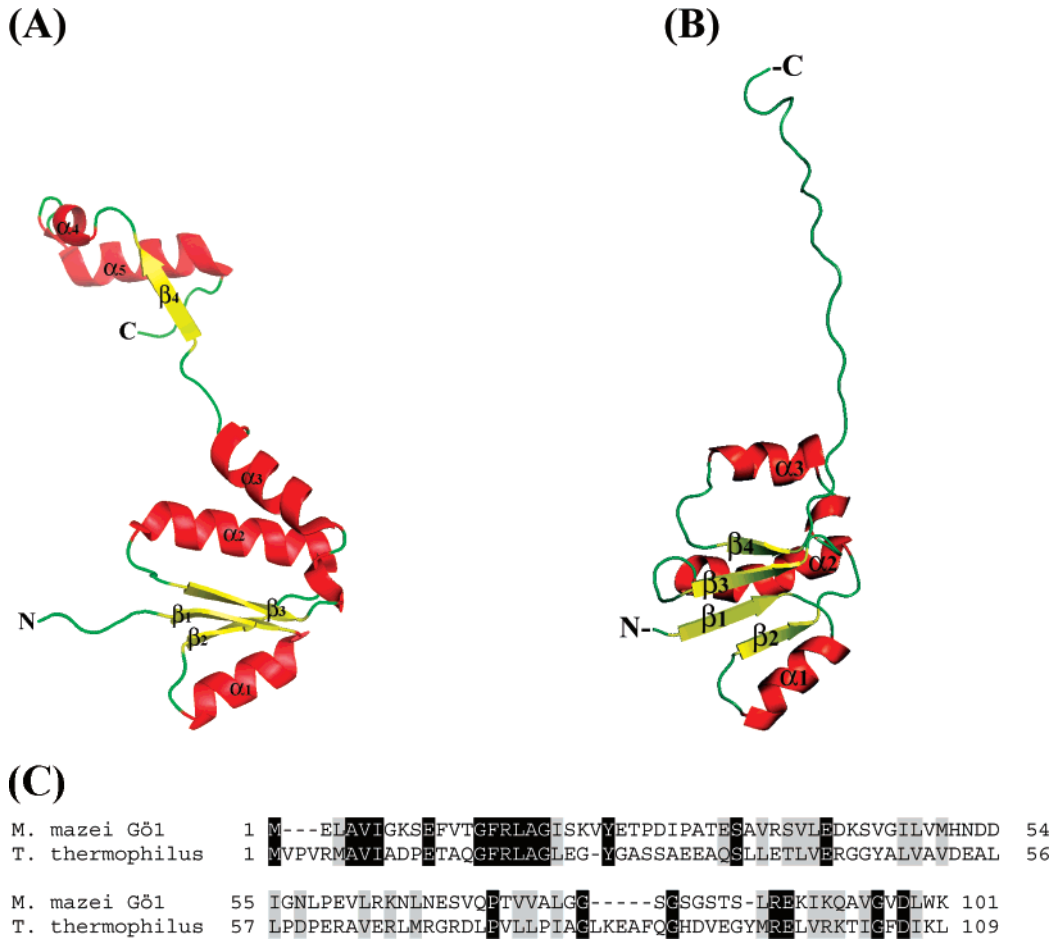

FIGURE 8: Ribbon representation of the F subunit of the bacterial V_1V_O ATPase from *T. thermophilus* (A) (PDB code 2D00; *24*) and F of the A_1A_O ATP synthase from *M. mazei* Gö1 (B), derived from crystallographic and NMR analysis. (C) Sequence and secondary structure alignment of subunit F of the prokaryotic V_1V_O ATPase from *T. Thermophilus* (*24*) and F of the A_1A_O ATP synthase from *M. mazei* Gö1. The identity (black) of both proteins is 19%. Alignment was generated using AlignX (Vector NTI v9 InforMax).

and A_1A_O ATP synthase (*12*), depending on whether MgATP or the nonhydrolyzable ATP analogue MgAMP-PNP is bound to the enzyme. The peptides involved in this EDC (1-ethyl-3-[(dimethylamino)propyl]carbodiimide)[1] induced zero-length cross-link of B and F are $_{390}$EALSERDTK$_{399}$, a sequence homologous to that of the so-called DELSEED region of F-ATP synthases (*18*), and $_{88}$REKIK$_{92}$ (*M. mazei* Gö1 numbering), respectively (*12*). The surface representation of subunit F (Figure 6) indicates the positively charged area of this sequence, forming the cross-link with one of the negatively charged residues of the C-terminus of subunit B. The size and specificity of the fluorescence response of Trp340 of subunit B upon binding of the F subunit mutant *F*W100Y (Figure 5A) clearly signify that it is the very C-terminal end of the stalk subunit F which also forms a contact area with the C-terminal region containing W430 of subunit B (Figure 7). Both peptides $_{390}$EALSERDTK$_{399}$ and $_{422}$IEDTLEIGWQ$_{431}$ of B belong to the C-terminal region (*9*), which in the nucleotide-binding subunit α of the related F_1F_O ATP synthases undergoes rotation after binding of nucleotides (*19*−*22*). Therefore, the close proximity of the sequences $_{88}$REKIK$_{92}$ and $_{98}$DLWK$_{101}$ of the C-terminus of subunit F and the C-terminal residues of B might induce a conformational change in the lower C-terminal region of B with the subsequent closing of the binding pocket. It has been shown recently that the B−F interaction is absent in the presence of MgADP + P_i or MgADP, due to a relative movement of subunit F (*12*). The high flexibility of F_{Mm} presented enables the subunit to undergo rearrangements during energy coupling as they are described for the proposed homologue ϵ of the *E. coli* F_1F_O ATP synthase (*23*) and subunit F (F_{Tt}) of the related prokaryotic V-ATPase from *Thermus thermophilus* (*24*).

There is also biochemical evidence that subunit F of the A-ATP synthase is in close contact with the rotating subunit D (*10*, *11*). The four-stranded *β*-sheet in the N-terminal part forms a hydrophobic surface (Figure 6B) that might mediate the interaction of both subunits (Figure 7). Such positioning of subunit D relative to subunit F is in line with the arrangement of the C-termini of subunits B and F as described above. Consequently, the positively and negatively charged surface of the bottom of the N-terminal domain of F would be oriented to the central stalk subunit C and thereby toward the membrane side. As described recently, subunits D, C, and F form a cross-linked product inside the A_1 ATPase (*10*, *11*), giving the central stalk a significant length of 84 Å (*7*).

With a globular part, made up by the N-terminal region, and a hooklike part, formed by the C-terminus, the three subunits F_{Tt}, ϵ, and F_{Mm} display the same overall appearance, although subunit F_{Mm} shows a sequence identity of 9% and 19% to subunits ϵ and F_{Tt}, respectively (*12*). However, the secondary and tertiary structures of these subunits are different. As shown in Figure 8A the N-terminal domain of

the crystallographic structure of F_{Tt} of the prokaryotic V-ATPase, determined at 2.2 Å resolution (*24*), is made up by an alternating arrangement of three β-strands (β1−3) and three α-helices (α1−3). By comparison, the global N-terminal part of subunit F (F_{Mm}) of the A_1A_O ATP synthase is composed of a four-stranded β-sheet, the strands of which, in contrast to the structure of F_{Tt}, are oriented parallel to each other, causing a hydrophobic surface (see above). Whereas helix 1 in both F subunit structures shows a similar orientation, helix 2 has different positions in the two structures, corresponding to a parallel orientation of this helix relative to β-strand 3 in the case of subunit F_{Mm}. There is also a significant difference between the positions of helix 3, which in the F_{Tt} structure becomes oriented to the direction of the elongated C-terminal part, whereas in subunit F_{Mm} helix 3 runs parallel above helix 2, forming together with β4 the upper part of the global N-terminal section. In addition, the C-terminal domain (residues 75−109) in the F_{Tt} structure consists of β-strand 3, followed by the short and long helices 4 and 5, respectively (*24*). In contrast, subunit F_{Mm} shows an extended tail at its very end. The structures F_{Tt} and F_{Mm} show a disordered region of residues 71−74 and 87−95, respectively, indicating structural flexibility of the C-terminal domain. The direct measurements of backbone dynamics including R_1, R_2, and two-dimensional $^1H-^{15}N$ heteronuclear NOE experiments of subunit F_{Mm} are consistent with this observation. The fact that the C-terminal domain is not completely ordered is not surprising, since many biological target peptides are poorly structured before complex formation. Many of these targets adopt a helical structure within the complex (*25*), and it is possible that a well-ordered structure is achieved when the F subunit binds a biological partner such as the B subunit.

From the dimer formation of F_{Tt} of the prokaryotic V-ATPase, in which the N-terminal domain of one monomer of F_{Tt} forms a globular fold together with the C-terminal domain of another monomer, it has been proposed that subunit F_{Tt} might exist in an extended and retracted form. Like in the related procaryotic V-ATPase the stoichiometry of subunit F (F_{Mm}) inside the A_1 ATPase (*10*) and the A_1A_O ATP synthase (*13*) is 1. The monomeric subunit F_{Mm} in solution, which has been studied by SAXS and nuclear magnetic resonance spectroscopy, is elongated. However, its flexible C-terminal tail enables this subunit to undergo up-and-down movements relative to its neighbor, the nucleotide-binding subunit B.

In summary, the first three-dimensional structure of the central stalk subunit F of the A-ATP synthase in solution provides the structural basis toward a fuller understanding of the mechanistical properties of this subunit inside this class of enzymes. Moreover, it gives more insight into the structural and thereby functional homologies and diversities of the coupling subunits ϵ, F_{Tt}, and F_{Mm} of the related prokaryotic F-ATP synthase and V-ATPase and the archaeal A-ATP synthase, respectively.

SUPPORTING INFORMATION AVAILABLE

Amino acid sequence of the F subunit (Figure S1), two-dimensional $^1H-^{15}N$ HSQC spectra of the F subunit with different peak shapes and intensities (Figure S2), one-dimensional projection of representative $^1H-^{15}N$ HSQC peaks of the F subunit (Figure S3), intensities of the HSQC cross-peaks as a function of residue position (Figure S4), and a schematic representation of the secondary structure (Figure S5). This material is available free of charge via the Internet at http://pubs.acs.org.

REFERENCES

1. Schäfer, G., Engelhard, M., and Müller, V. (1999) Bioenergetics of the archaea, *Mol. Biol. Rev. 63*, 570−620.
2. Müller, V., Lingl, A., Coskun, Ü., and Grüber, G. (2005) Functional and structural modules of the A-type ATP synthase, *J. Mol. Microbiol. Biotechnol. 10*, 167−180.
3. Weber, J., and Senior, A. E. (2003) ATP synthesis driven by proton transport in F_1F_0-ATP synthase, *FEBS Lett. 545*, 61−70.
4. Forgac, M. (2000) Structure, mechanism and regulation of the clathrin-coated vesicle and yeast vacuolar H(+)-ATPases, *J. Exp. Biol. 203*, 71−80.
5. Lolkema, J. S., Chaban, Y., and Boekema, E. J. (2003) Subunit composition, structure, and distribution of bacterial V-type ATPase, *J. Bioenerg. Biomembr. 35*, 323−336.
6. Müller, V., and Grüber, G. (2003) ATP syntases: structure, function and evolution of unique energy converters, *Cell Mol. Life Sci. 60*, 474−494.
7. Grüber, G., Svergun, D. I., Coskun, Ü., Lemker, T., Koch, M. H. J., Schägger, H., and Müller, V. (2000) Structural insights into the A_1 ATPase from the archaeon, *Methanosarcina mazei* Gö1, *Biochemistry 40*, 1890−1896.
8. Maegawa, Y., Morita, H., Iyaguchi, D., Yao, M., Watanabe, N., and Tanaka, I. (2006) Structure of the catalytic nucleotide-binding subunit A of A-type ATP synthase from *Pyrococcus horikoshii* reveals a novel domain related to the peripheral stalk, *Acta Crystallogr. D62*, 483−488.
9. Schäfer, I., Bailer, S. M., Düser, M. G., Börsch, M., Ricardo, A. B., Stock, D., and Grüber, G. (2006) Crystal structure of the archaeal A_1A_O ATPsynthase subunit B from *Methanosarcina mazei* Gö1: Implications of nucleotide-binding differences in the major A_1A_O subunits A and B, *J. Mol. Biol. 358*, 725−740.
10. Coskun, Ü., Radermacher, M., Müller, V., Ruiz, T., and Grüber, G. (2004) Three-dimensional organization of the archaeal A_1-ATPase from *Methanosarcina mazei* Gö1, *J. Biol. Chem. 279*, 22759−22764.
11. Coskun, Ü., Grüber, G., Koch, M. H. J., Godovac-Zimmermann, J., Lemker, T., and Müller, V. (2002) Cross-talk in the A1-ATPase from *Methanosarcina mazei* Gö1 due to nucleotide binding, *J. Biol. Chem. 277*, 17327−17333.
12. Schäfer, I., Rössle, M., Biuković, G., Müller, V., and Grüber, G. (2006) Structural and functional analysis of the coupling subunit F in solution and topological arrangement of the stalk domains of the methanogenic A_1A_O ATPsynthase, *J. Bioenerg. Biomembr. 38*, 83−92.
13. Coskun, Ü., Chaban, Y. L., Lingl, A., Müller, V., Keegstra, W., Boekema, E. J., and Grüber, G. (2004) Structure and subunit arrangement of the A-type ATP synthase complex from the archaeon *Methanococcus jannaschii* visualized by electron microscopy, *J. Biol. Chem. 279*, 38644−38648.
14. Bernal, R. A., and Stock, D. (2004) Three-dimensional structure of the intact *Thermus thermophilus* H+-ATPase/synthase by electron microscopy, *Structure 12*, 1789−1798.
15. Lokanath, N. K., Matsuura, Y., Kuroishi, C., Takahashi, N., and Kunishima, N. (2006) Dimeric core structure of modular stator subunit E of archaeal H^+-ATPase, *J. Mol. Biol. 366*, 933−944.
16. Biuković, G., Rössle, M., Gayen, S., Mu, Y., and Grüber, G. (2007) Small-angle X-ray scattering reveals the solution structure of the peripheral stalk subunit H of the A_1A_O ATP synthase from *Methanocaldococcus jannaschii* and its binding to the catalytic A subunit, *Biochemistry 46*, 2070−2078.
17. Wilms, R., Freiberg, C., Wegerle, E., Meier, I., Mayer, F., and Müller, V. (1996) Subunit structure and organization of the genes of the A_1A_O ATPase from the archaeon *Methanosarcina mazei* Gö1, *J. Biol. Chem.* 271, 18843−18852.
18. Gibbons, C., Montgomery, M. G., Leslie, A. G., and Walker, J. E. (2000) The structure of the central stalk in bovine F(1)-ATPase at 2.4 A resolution, *Nat. Struct. Biol. 7*, 1055−1061.
19. Aggeler, R., Grüber, G., and Capaldi, R. A. (1998) Trapping of conformations of the *Escherichia coli* F_1 ATPase by disulfide bond

formation. A state of the enzyme with all three catalytic sites open and with equal low affinity for nucleotides, *FEBS Lett. 426*, 37−40.
20. Menz, R. I., Walker, J. E., and Leslie, A. G. W. (2001) Structure of bovine mitochondrial F_1-ATPase with nucleotide bound to all three catalytic sites: Implications for the mechanism of rotary catalysis, *Cell* 106, 331−341.
21. Kabaleeswaran, V., Puri, N., Walker, J. E., Leslie, A. G. W., and Mueller, D. M. (2006) Novel features of the rotary catalytic mechanism revealed in the structure of yeast F_1 ATPase, *EMBO J. 25*, 5433−5442.
22. Feniouk, B. A., Suzuki, T., and Yoshida, M. (2006) The role of subunit epsilon in the catalysis and regulation of F_OF_1-ATP synthase, *Biochim. Biophys. Acta 1757*, 326−338.
23. Wilkens, S., Dahlquist, F. W., McIntosh, L. P., Donaldson, L. W., and Capaldi, R. A. (1995) Structural features of the epsilon subunit of the *Escherichia coli* ATP synthase determined by NMR spectroscopy, *Nat. Struct. Biol. 2*, 961−967.
24. Makyio, H., Iino, R., Ikeda, C., Imamura, H., Tamakoshi, M., Iwata, M., Stock, D., Bernal, R. A., Carpenter, E. P., Yoshida, M., Yokoyama, K., and Iwata, S. (2005) Structure of a central stalk subunit F of prokaryotic V-type ATPase/synthase from *Thermus thermophilus*, *EMBO J. 24*, 3974−3983.
25. Crivici, A., and Ikura, M. (1995) Molecular and structural basis of target recognition by calmodulin, *Annu. Biophys. Biomol. Struct. 24*, 85−116.
26. Laemmli, U. K. (1970) Cleavage of structural proteins during the assembly of the head of bacteriophage T4, *Nature 227*, 680−685.
27. Kneller, D. G., and Goddard, T. D. (1997) SPARKY, 3.105 ed., University of California, San Francisco, CA.
28. Wüthrich, K. (1986) *NMR of Proteins and Nucleic Acids*, Wiley, New York.
29. Cornilescu, G., Delaglio, F., and Bax, A. (1999) Protein backbone angle restraints from searching a database for chemical shift and sequence homology, *J. Biomol. NMR 13*, 289−302.
30. Wishart, D. S., Sykes, B. D., and Richards, F. M. (1992) The chemical shift index: a fast and simple method for the assignment of protein secondary structure through NMR spectroscopy, *Biochemistry 31*, 1647−1651.
31. Guntert, P., Mumenthaler, C., and Wüthrich, K. (1997) Torsion angle dynamics for NMR structure calculation with the new program DYANA, *J. Mol. Biol. 273*, 283−298.
32. Herrmann, T., Guntert, P., and Wüthrich, K. (2002) Protein NMR structure determination with automated NOE assignment using the new software CANDID and the torsion angle dynamics algorithm DYANA, *J. Mol. Biol. 319*, 209−227.
33. Koradi, R., Billeter, M., and Wüthrich, K. (1996) MOLMOL: a program for display and analysis of macromolecular structures, *J. Mol. Graphics 14*, 51−55.
34. Shaka, A. J., Barker, P. B., and Freeman, R. (1985) Computer-optimized decoupling scheme for wideband applications and low-level operation, *J. Magn. Reson. 64*, 547−552.
35. Pervushin, K., Wider, G., and Wüthrich, K. (1997) Deuterium Relaxation in a uniformly ^{15}N labelled homeodomain and its DNA complex, *J. Am. Chem. Soc. 119*, 3842−3843.
36. Loria, J. P., Rance, M., and Palmer, A. G. (1999) A relaxation-compensated Carr-Purcell-Meiboom-Gill sequence for characterizing chemical exchange by NMR spectroscopy, *J. Am. Chem. Soc. 121*, 2331−2332.
37. Gallopin, M., Ochsenbein, F., Guittet, E., and Heijenoort, C. V. (2004) Analysis of slow motions in the micro−millisecond range on domain 1 of annexin I, *C. R. Acad. Sci., Ser. IIc: Chim. 7*, 253−258.
38. Delaglio, F., Grzesiek. S., Vuister, G. W., Zhu, G., Pfeifer, J., and Bax, A. (1995) NMRPipe: a multidimensional spectral processing system based on UNIX, *J. Biomol. NMR 6*, 277−293.
39. Kneller, D. G., and Goddard, T. D. (1997) SPARKY, 3.105 ed., University of California, San Francisco, CA.
40. Cavanagh, J. (1996) Referencing, *Protein NMR spectroscopy: Principles and practice*, p 175, Academic Press, San Diego.
41. Farrow, N. A., Muhandiram, R., Singer, A. U., Pascal, S. M., Kay, C. M., Gish, G., Shoelson, S. E., Pawson, T., Forman-Kay, J. D., and Kay, L. E. (1994) Backbone dynamics of a free and phosphopeptide-complexed Src homology 2 domain studied by ^{15}N NMR relaxation, *Biochemistry 33*, 5984−6003.
42. Merritt, E. A., and Murphy, M. E. (1997) Raster3D Version 2.0. A program for photorealistic molecular graphics, *Acta Crystallogr. D50*, 869−873.
43. Gibbons, C., Montgomery, M. G., Leslie, A. G., and Walker, J. E. (2000) The structure of the central stalk in bovine F(1)-ATPase at 2.4 A resolution, *Nat. Struct. Biol. 7*, 1055−1061.

BI701102N